

P007 PULSE STRETCH EFFECTS IN THE CONTEXT OF DATA-DRIVEN IMAGING METHODS

J. MANN and G. HÖCHT
Geophysical Institute, University of Karlsruhe, Hertzstr. 16, 76187 Karlsruhe, Germany

Summary. Moveout corrections based on hyperbolic traveltime approximations are usually expected to cause distortions of the wavelet, especially for comparatively small traveltimes and large offsets. This kind of pulse stretch effect is well known from the conventional NMO correction and requires appropriate muting of the pre-stack data before stacking. However, data-driven imaging methods based on multi-parameter traveltime approximations like Multifocusing, delayed hyperbola approaches, or Common-Reflection-Surface (CRS) stack do not expose such a stretch phenomenon. We briefly review the origin of the pulse stretch effect and relate it to the artificial smoothness of typically applied NMO velocity fields. Data-driven imaging methods like CRS stack introduce a systematic variation of the stacking velocity to avoid the unwanted pulse stretch. In contrast, the associated kinematic CRS wavefield attributes remain virtually constant and turn out to be a more appropriate parameterization of the recorded wavefield.

Introduction. Conventional imaging methods often systematically distort the wavelet with respect to its length and its shape, leading to a reduced frequency content and the risk of misinterpretation. These effects occur even if the stacking operators are kinematically correct: they are due to the usually smooth parameterization of the model. This kind of unwanted changes of the wavelet do not occur during the CRS stack and similar data-oriented imaging methods like Multifocusing (Berkovitch et al., 1994; Landa et al., 1999) or the delayed hyperbola approaches by de Bazelaire (1988); Thore et al. (1994). To explain this fact, we briefly review the reasons for the pulse stretch in conventional imaging methods for a simple example where the respective stacking operators are kinematically exact. We discuss different approximations for the stacking trajectories for neighboring samples along the wavelet in band-limited data and compare them to the stacking velocities determined by means of the CRS stack. It turns out that the optimum stacking velocity model is not smooth but reveals a systematic variation of the stacking velocity along the wavelet. Reformulated in terms of kinematic wavefield attributes, these variations can be removed to a large extent and allow a more reliable extraction of information for subsequent processing steps like inversion.

CMP traveltimes along the wavelet. Pulse stretch even occurs for events with perfectly hyperbolic traveltime curves. To focus on this effect, we only investigate such idealized situations in the following. For the sake of simplicity, we consider the simplest situation, a plane horizontal reflector with homogeneous overburden. For a reflector at depth z_0 and a velocity v_0 , the kinematic reflection response is given by

$$t(h) = \frac{2}{v_0} \sqrt{h^2 + z_0^2} = \sqrt{t_0^2 + \frac{4h^2}{v_0^2}}, \quad (1)$$

where $t_0 = 2z_0/v_0$ denotes the zero-offset (ZO) traveltime and h is the half-offset. For a medium without attenuation, the pre-stack data can be represented as a convolution of the wavelet and the kinematic reflection response (phase shifts are not considered here): the pulse length is identical for all shot and receiver locations. An undistorted result can be obtained by stacking along the kinematic reflection response (1)

vertically shifted by Δt to all locations within the wavelet of length T :

$$t(h, \Delta t) = \sqrt{t_0^2 + \frac{4h^2}{v_0^2}} + \Delta t \quad \text{with} \quad -\frac{T}{2} \leq \Delta t \leq \frac{T}{2}, \quad (2)$$

where we assume that the wavelet is centered around the traveltimes t . An NMO correction applied with the velocity v_0 yields the correct traveltimes for the center of the wavelet. However, the NMO operator attached to a neighboring ZO traveltimes differs from the corresponding iso-phase curve (2). The time shift between two NMO operators with the same stacking velocity but attached to different ZO traveltimes is not constant but decreases with increasing offset. This leads to the pulse stretch effect.

Alternative approximation of the stacking velocity. Obviously, a constant stacking velocity model is not suited to describe the iso-phase curves in the input data, not even in the simplest possible situation: a more appropriate description of the stacking velocity along the seismic wavelet is required. If we express the shifted hyperbola (2) in the same form as the hyperbolic operator (1) and in terms of the ZO traveltimes t_0 and the velocity v_0 defined at the center of the wavelet, we obtain a new stacking velocity:

$$v_{\text{shift}}^2(\Delta t, h) = \frac{2h^2 v_0^2}{2h^2 + v_0^2 \Delta t \sqrt{t_0^2 + \frac{4h^2}{v_0^2}} - v_0^2 t_0 \Delta t}. \quad (3)$$

This velocity explicitly depends on h , in other words, the shifted hyperbola (2) cannot be expressed by means of a single stacking velocity. For an exact description of the iso-phase curves in the data, we would have to allow an additional parameter, the time shift Δt itself. To avoid this additional parameter, a reasonable approximation of v_{shift} is required. In conventional processing, v_{shift} is assumed to coincide with v_0 , which only holds for $h \rightarrow \infty$. For the simulation of ZO sections, a more reasonable approach is to require a constant curvature at offset zero of all stacking hyperbolae. The corresponding stacking velocity reads

$$v_{\text{shift,c}}^2(\Delta t) = \frac{t_0}{t_0 + \Delta t} v_0^2. \quad (4)$$

Numerical example for a 1-D model. To analyze the behavior of the stacking velocity derived by means of the CRS stack method, we defined a simple 1-D model consisting of three horizontal reflectors at depths $z_i = 1000, 1080, 1160$ m with a constant velocity $v_0 = 1500$ m/s such that all events are perfectly hyperbolic. A CMP gather with half-offsets up to 500 m was simulated with a fold of 31 and a Ricker wavelet with 30 Hz peak frequency. Some noise was added to avoid artifacts during the CRS processing. The modeled ZO trace is shown on the left-hand side of Figure 1a. The CMP gather served as input to the first step of the CRS stack processing scheme, the automatic CMP stack. This process also uses the one-parameter operator (1). However, it determines the optimum stacking velocity separately for each simulated ZO sample without imposing any smoothness. The resulting stacked trace is shown on the right-hand side of Figure 1a: the wavelet is recovered without any stretch. The associated coherence values calculated along the stacking trajectories are depicted in Figure 1b. The detected stacking velocity is shown as solid line in Figures 1c and d. As expected from the considerations in the previous section, it is not constant along the wavelet, but exposes a characteristic ‘‘jig saw’’ appearance: it *decreases* along the wavelet with *increasing* traveltimes. Let us now compare the detected velocity to the expected behavior for constant ZO curvature according to Equation (4). The analytic values are displayed as dashed lines in Figure 1c, of course separately for each event. We observe a very good fit to the semblance-based results extracted from the pre-stack data. Let us go a step further: the assumption of constant curvature only provides a constant time shift close to offset zero. However, a finite half-offset range of 0...500 m contributes to the stack. Thus, one might argue that Equation (3) might provide an even better fit for a certain ‘‘average offset’’ such that the deviation from the constant time shift is as small as possible for all given offsets. We analyzed this by minimizing the least square error between the shifted hyperbolae and its one-parameter approximation. The result is very similar to the constant curvature approach shown in Figure 1d and fits the detected velocities even slightly better.

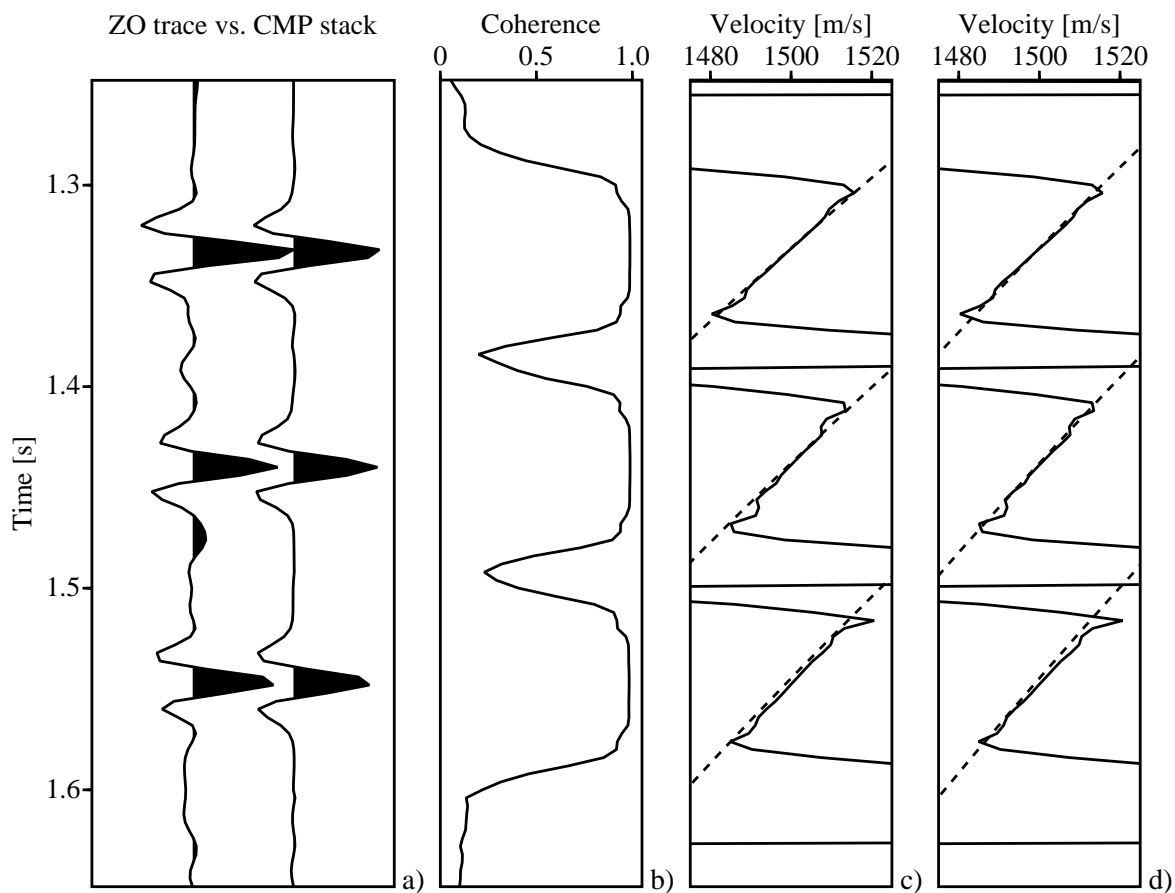


Figure 1: Synthetic example: a) slightly noisy modeled ZO trace vs. the automatic CMP stack result, b) coherence measure semblance calculated along the stacking hyperbolae, c) detected stacking velocities (solid line) vs. forward-calculated stacking velocities (dashed lines) for hyperbolae with the same curvature at offset zero, and d) same as c) but for hyperbolae providing the best kinematic fit within the given offset range.

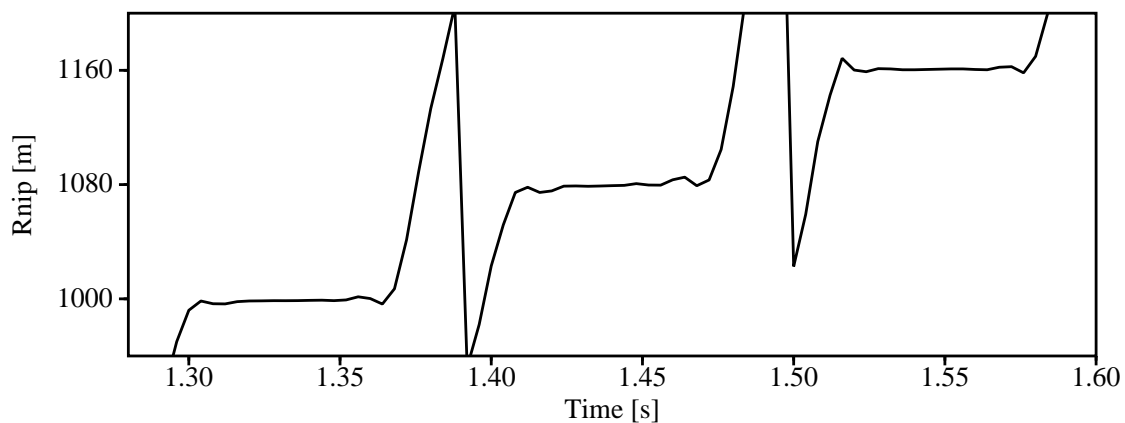


Figure 2: Synthetic example: radius of the NIP wavefront. In contrast to the stacking velocity, R_{NIP} is almost constant along the wavelet and—for this simple model—represents the reflector depths $z_i = 1000, 1080, 1160$ m.

Behavior of the kinematic wavefield attributes. In the following, we will reformulate the preceding sections in terms of the CRS wavefield attributes. The CRS operator is also a hyperbolic representation and its shape also explicitly depends on the ZO traveltime t_0 . Expressed in terms of midpoint coordinate x_m and half-offset h , it reads

$$t_{\text{hyp}}^2(x_m, h) = \left[t_0 + \frac{2 \sin \alpha (x_m - x_0)}{v_0} \right]^2 + \frac{2 t_0 \cos^2 \alpha}{v_0} \left[\frac{(x_m - x_0)^2}{R_N} + \frac{h^2}{R_{\text{NIP}}} \right], \quad (5)$$

where v_0 represents the near-surface velocity and (t_0, x_0) is the considered ZO location. The CRS operator is parameterized by three kinematic wavefield attributes defined at the surface location x_0 , namely α , the emergence angle of the normal ray, R_{NIP} , the radius of the normal-incidence-point (NIP) wavefront, and R_N , the radius of the normal wavefront. The relation of these attributes to two so-called eigenwave experiments can, e. g., be found in Jäger et al. (2001). For the considered 1-D model, all rays are vertical and all normal wavefronts are plane, i. e., $\alpha = 0$ and $R_N = \pm\infty$ for all three events. Accordingly, the CRS operator reduces to

$$t(h) = \sqrt{t_0^2 + \frac{2 t_0 h^2}{v_0 R_{\text{NIP}}}} \quad (6)$$

for any midpoint location x_m . For the center of the wavelet, this represents the exact kinematic reflection response of the reflector with $R_{\text{NIP}} = z_i$. This is an alternative formulation of the CMP moveout formula (1). Reformulating Eq. (4) in terms of R_{NIP} we readily observe that R_{NIP} remains constant along the wavelet. This is equivalent to the assumption of constant ZO curvature. Indeed, the NIP wavefront radius (Figure 2) is almost constant for each event. This radius appears to be a more natural parameter for the traveltime curves. So far, we only considered the CMP gather. As the CRS operator is hyperbolic for any configuration that includes the simulated ZO location, e. g., common-shot or common-receiver gather or the ZO section, the same behavior is expected in any case. The additional linear term in any gather except the CMP gather does not change the principal properties. The respective radius of curvature, in general a linear combination of $1/R_{\text{NIP}}$ and $1/R_N$, will remain almost constant along the wavelet and the pulse stretch will be avoided.

Conclusions. We briefly reviewed the origin of pulse stretch in conventional time domain processing with constant or smooth NMO velocity models. A stretch free imaging with optimally recovered wavelet is not possible with such models. We discussed an approximation of the stacking velocity variation along the wavelet that is better suited for the simulation of ZO sections. A comparison with CRS stack results for a 1-D model demonstrated that data-driven imaging methods automatically avoid the pulse stretch and introduce a systematic variation of the stacking velocity. Formulated in terms of the kinematic CRS wavefield attributes, this variation vanishes. Thus, the radii of wavefront curvatures involved in the CRS stack approach provide a more appropriate parameterization of the reflection events.

Acknowledgments

We would like to thank the sponsors of the *Wave Inversion Technology Consortium* for their support.

References

- Berkovitch, A., Gelchinsky, B., and Keydar, S. (1994). Basic formulae for multifocusing stack. In *Extended Abstracts*. 56th Mtg. Eur. Assoc. Expl. Geophys. Session: P140.
- de Bazelaire, E. (1988). Normal moveout revisited – inhomogeneous media and curved interfaces. *Geophysics*, 53(2):143–157.
- Jäger, R., Mann, J., Höcht, G., and Hubral, P. (2001). Common-reflection-surface stack: Image and attributes. *Geophysics*, 66(1):97–109.
- Landa, E., Gurevich, B., Keydar, S., and Trachtman, P. (1999). Application of multifocusing method for subsurface imaging. *J. Appl. Geoph.*, 42(3,4):283–300.
- Thore, P. D., de Bazelaire, E., and Ray, M. P. (1994). Three-parameter equation: An efficient tool to enhance the stack. *Geophysics*, 59(2):297–308.